

# Tripartite GHZ Entanglement in Monitored Random Clifford Circuits

Guanglei Xu<sup>1</sup> and Yu-Xiang Zhang<sup>1,2,3,\*</sup>

<sup>1</sup>*Institute of Physics, Chinese Academy of Sciences, Beijing 100190, China*

<sup>2</sup>*School of Physical Sciences, University of Chinese Academy of Sciences, Beijing 100049, China*

<sup>3</sup>*Hefei National Laboratory, Hefei, 230088, China*

(Dated: July 4, 2024)

Multipartite quantum entanglement of a manybody is not well understood. Here we numerically study the amount of tripartite Greenberger-Horne-Zeilinger (GHZ) states that can be extracted from the state generated by random Clifford circuits with probabilistic single-qubit projective measurements. We find a GHZ-entangled phase where this amount is finite and a GHZ-trivial phase where no tripartite entanglement is available. The transition between them is either measurement-induced, at  $p_c \approx 0.16$ , or partition-induced when a party contains more than half of the qubits. We find that the GHZ entanglement can be enhanced by measurements in certain regimes, which could be understood from the perspective of quantum Internet. Effects of the measurements to the growth of GHZ entanglement are also studied.

There are countless inequivalent ways in which particles of a manybody system can be entangled. However, only bipartite quantum entanglement is relatively well-understood [1–3]. Bipartite entanglement omits all the complexities within the same party, resulting in a vastly coarse-grained description. Despite that, nontrivial features have already emerged at this level, particularly a transition between phases with area-law and volume-law bipartite entanglement [4–7]. Recently, this transition has also been observed in random circuits where qubits arranged in a one-dimensional (1D) layout undergo random two-qubit unitaries intercepted with probabilistic single-qubit projective measurements [8–12]. Entanglement transition in this system has been mapped to a classical statistical mechanics model of Potts-like spins [13–15]. The growth of bipartite entanglement entropy in the volume-law phase can be understood from entanglement domain walls [16, 17] and directed polymer in a random environment [18]. Monitored 1D random circuits have become a high-profile platform for studying the interplay between information-theoretical concepts and quantum manybody dynamics. Recent works have also extended the systems to circuits with long-range gates [19–21], multi-qubit measurements [22, 23], other dimensions [24–28] spacetime duality [29–31], error correction properties [32–35], noisy circuits [36–38] and experiments [39], etc.

Considering these substantial discoveries and the significant gap between the coarse-grained bipartite descriptions and the finest multipartite structures, we are motivated to advance to tripartite entanglement, for which only a few results are available [40, 41] in the context of manybody systems. As illustrated in Fig. 1(a), we accommodate ourselves by restricting the random two-qubit gates to the *Clifford* group. The problem is simplified for two reasons. Firstly, Clifford circuits can be simulated efficiently [42–44]. Secondly, states generalized by Clifford circuits, the *stabilizer states*, has a clear structure of tripartite entanglement. Namely, up to uni-

ties localized in each party, a stabilizer state  $|\Psi\rangle_{ABC}$  is equivalent to a collection of isolated single-qubit states, two-qubit Bell states  $|\psi\rangle = (|00\rangle + |11\rangle)/\sqrt{2}$  and three-qubit GHZ states  $|\text{GHZ}\rangle = (|000\rangle + |111\rangle)/\sqrt{2}$  [45], cf. Fig. 1(b). Neglecting the isolated qubits that are irrelevant to entanglement, the equivalence reads:

$$|\Psi\rangle_{ABC} \sim |\psi\rangle_{AB}^{\otimes n_{AB}} \otimes |\psi\rangle_{BC}^{\otimes n_{BC}} \otimes |\psi\rangle_{AC}^{\otimes n_{AC}} \otimes |\text{GHZ}\rangle_{ABC}^{\otimes g}. \quad (1)$$

The index  $g$ , which counts the entanglement of the GHZ type [46], will be the focus of this Letter. It should *not* be confused with the notion of genuinely multipartite entanglement [1, 47], which is referred to states cannot be prepared by a mixture of product states in the form of  $\rho_A \otimes \rho_{BC}$ ,  $\rho_B \otimes \rho_{AC}$  and  $\rho_C \otimes \rho_{AB}$ . This notion does not exclude the Bell states contained in Eq. (1).

The index  $g$  is typically small for stabilizer states [48] and stabilizer tensor networks [41], see also an estima-

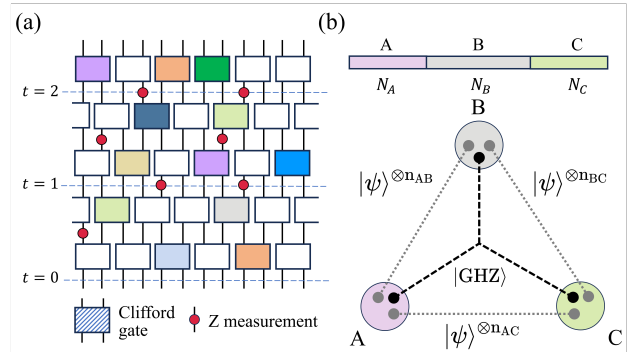


Figure 1. (a) Schematic of the setup: Random Clifford gates implemented upon neighboring qubits are arranged in a brickwork configuration. Each layer of the circuits consists of two levels of random unitaries and after each level, projective Z-measurements are applied independently to every qubit with probability  $p$ . (b) Illustration of the tripartite decomposition of a stabilizer state into Bell pairs  $|\psi\rangle$  and the GHZ state  $|\text{GHZ}\rangle$  omitting isolated single qubits.

tion in [49]. However, having few in numbers does not mean lacking of features. We find that the monitored random Clifford circuits exhibit a GHZ-entangled phase where  $g$  is finite and a GHZ-trivial phase where  $g$  vanishes. The transition between them can be either measurement-induced, at the measurement probability  $p \approx 0.16$  which is close to (if not identical to) the critical point of the bipartite entanglement transition [8, 10] and the purification phase transition [50], or *partition-induced*, which might be unique to multipartite entanglement. Throughout this Letter, we consider the geometry shown in Fig. 1(b), where each party is simply connected. The open boundary condition is assumed unless stated otherwise. We also assume that A and C have the same number of qubits. Thus, the way of partition is fixed by the ratio  $N_B/N$ . We find that the GHZ-entangled phase appears only when  $N_B/N < 1/2$ . Indeed, partition itself does not alter the underlying many-body state. It indicates an unexplored fundamental limit to the extent of multipartite entanglement established by local interactions.

Additionally, we also find that GHZ entanglement can be *enhanced* by measurements, contrasting with the negative impact on bipartite entanglement. The growth of  $g$  is studied with a comparison to the long-range bipartite entanglement.

*Preliminaries.* As shown in Fig. 1(a), we investigate the dynamics of 1D array of  $N$  qubits governed by random Clifford gates arranged in a brickwork configuration, intercepted by single-qubit measurement of Pauli  $Z$  operator with a probability of  $p$ . In our simulation, each circuit comprises  $N$  layers and each layer consists of two levels of random gates. The specific realization of all random Clifford gates and the outcomes of the probabilistic measurements determine a trajectory of state evolution. Our numerical results of  $\langle g \rangle$  are obtained by averaging 400 trajectories.

We initialize the qubits in  $|0\rangle$ , an eigenstate of the Pauli  $Z$  operator ( $Z|0\rangle = |0\rangle$ ). The initial state is a stabilizer state with the stabilizers  $\{Z_1, Z_2, \dots, Z_N\}$  [22]. Tracking the state evolution is equivalent to updating the set of stabilizers [42]. By the definition of Clifford gates, the stabilizers are always a product of the identity operator  $\mathbb{I}$  and the standard Pauli operators  $X, Y, Z$ . A stabilizer is said to act trivially on some qubit if the corresponding factor is  $\mathbb{I}$ . To compute  $g$ , one needs to identify a space (denoted by  $\mathcal{S}$ ) generated by all  $N$  stabilizers, following the rule that if  $s_1$  and  $s_2$  are both in  $\mathcal{S}$ , then  $s_1 s_2$  also belongs to  $\mathcal{S}$ . The space  $\mathcal{S}$  has three subspaces denoted by  $S_{\hat{\alpha}}$  for  $\alpha \in \{A, B, C\}$ , where  $S_{\hat{\alpha}}$  contains all elements of  $\mathcal{S}$  that act trivially on Party- $\alpha$ . Then, it has been proven that [45, 46]

$$g = N - \dim(\cup_{\alpha} S_{\hat{\alpha}}). \quad (2)$$

We simulate the circuits using QISKIT software packages to track the  $N \times 2N$  tableau to the binary representations

of the stabilizers [51]. All indices of Eq. (1) are obtained accordingly [49].

*Phase transitions.* We start with an equal partition,  $N_A=N_B=N_C=N/3$ , and calculate the average value  $\langle g \rangle$  for  $N = 120 \sim 240$  (in increments of 30). The results are plotted as a function of  $p$  in Fig. 2(a). It shows that  $\langle g \rangle$  is a finite value, insensitive to  $N$ , but changes with  $p$  abruptly in the interval  $0.1 < p < 0.2$ . The larger  $N$  is, the steeper the decline of  $\langle g \rangle$ . Thus, we anticipate a *measurement-induced* continuous transition of  $\langle g \rangle$ . In the inset of Fig. 2(a), we attempt a data collapse with the scaling form  $\langle g \rangle = F[(p - p_c)N^{1/\nu}]$  with  $F$  being an arbitrary function and  $\nu$  a critical exponent, and find that  $p_c \approx 0.159 \pm 0.002$  and  $\nu \approx 1.36$ . We refer to the phase for  $p < p_c$  as *GHZ-entangled* and the phase for  $p > p_c$  as *GHZ-trivial*. The critical point  $p_c$  aligns with those of the measurement-induced bipartite entanglement transition [8, 10] and the purification transition [50]. It is worth noting that  $\nu$  may not be universal, though we have not reached a conclusive dependence on  $N_B/N$ .

Perhaps surprisingly, we find that the critical mutual information displayed in Fig. 7 of an early work on the bipartite entanglement transition [52], is actually contributed by the tripartite GHZ entanglement [49]. The geometry used there is different: The periodic boundary condition is applied and one of the three party is not simply connected.

The dependence of  $\langle g \rangle$  on  $p$  changes significantly when we extend the size of B from  $N/3$  to  $8/15N$ , as shown in Fig. 2(b). Instead of the plateau observed in the GHZ-entangled phase, we see  $\langle g \rangle$  grows with  $p$  in a wide region of  $p < 0.15$ , demonstrating an enhancement induced by measurements. The striking difference between Figs. 2(a) and (b) prompts us to scan  $\langle g \rangle$  over both  $p$  and  $N_B/N$  in Fig. 2(c), for the case of  $N = 240$ . Values of  $g$  are represented by color mapping. The zigzags of the contours are due to statistical errors. Nevertheless, the plot demonstrates a clear plateau of  $\langle g \rangle > 1$ . Moreover, dense color changes, indicating ‘‘cliffs’’ of  $\langle g \rangle$ , are observed near the contours of  $\langle g \rangle = 0.4$  and  $0.7$ . These two contours are adjacent to the vertical line of  $p_c \approx 0.16$  and the horizontal line of  $N_B/N = 1/2$ . The former coordinates the measurement-induced transition, suggesting that the latter may imply another.

To learn Fig. 2(c) better, we analyze its vertical sections by plotting  $\langle g \rangle$  as a function of  $N_B/N$  for given values of  $p$  in Fig. 2(d). It manifests a congruence of the red curves ( $p < 0.16$ ) near  $N_B/N = 1/2$ . Then, we collect the curves of  $\langle g \rangle$  for  $p = 0$  and  $p = 0.08 \approx p_c/2$  across five different values of  $N$  in Figs. 2(e,f). Both figures exhibit curve crossings similar to those in Fig. 2(a). We attempt data collapse with the scaling form  $\langle g \rangle = G[(N_B/N - 1/2)N^{1/\mu}]$ , where  $G$  an arbitrary function, and show the result in the insets of Figs. 2(e, f). The critical indices are found to be  $\mu_0 = 1.011$  and  $\mu_{0.08} = 1.356$ . Thus, we believe there is a phase transi-

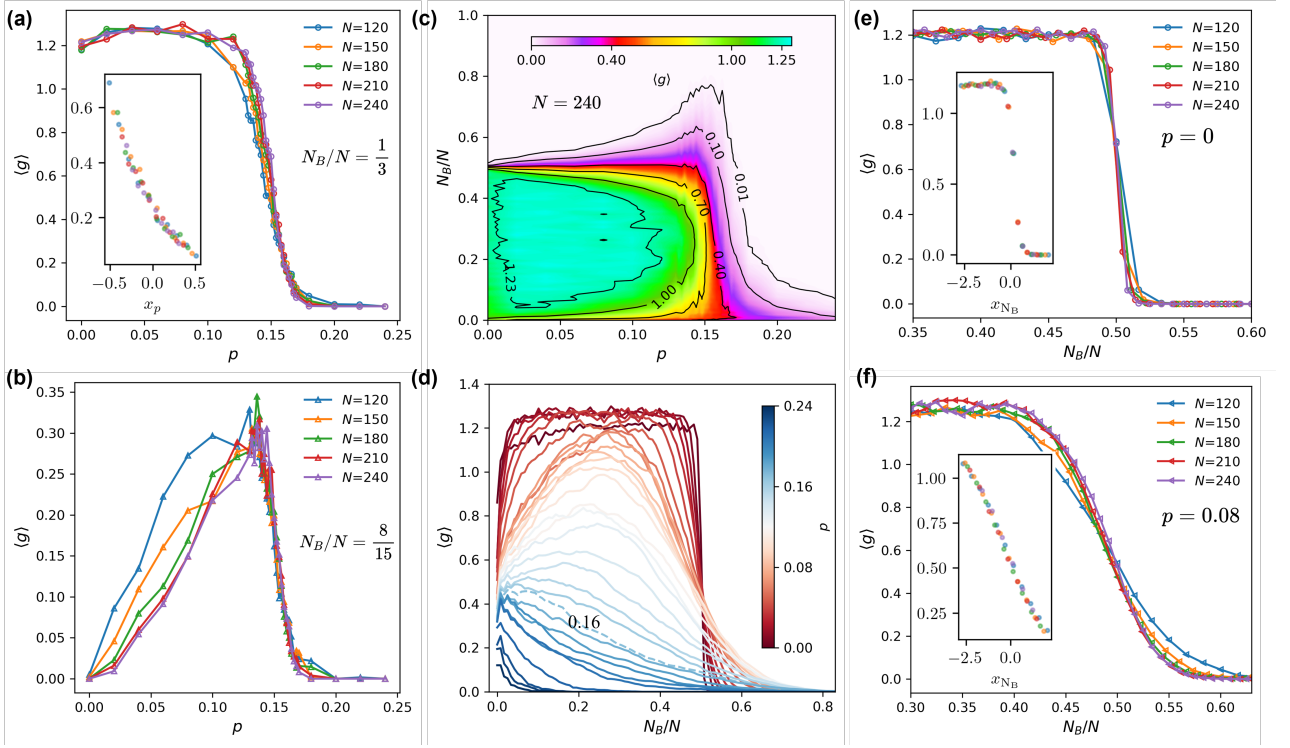


Figure 2. Measurement-induced and partition-induced entanglement transition. (a,b)  $\langle g \rangle$  as a function of  $p$  for the partition that  $N_B/N = 1/3$  in (a) and  $8/15$  in (b). The inset of (a) demonstrates the data collapse result, where the horizontal axis label is  $x_p \equiv (p - p_c)L^{1/\nu}$  and  $p_c \approx 0.16$ . (c)  $\langle g \rangle$  as a function of  $p$  and  $N_B/N$  for  $N = 240$ . (d)  $\langle g \rangle$  as a function of  $N_B/N$  for  $N = 240$  and a series of  $p$ . (e,f)  $\langle g \rangle$  as a function of  $N_B/N$  for  $p = 0$  in (e) and  $0.08$  in (f). The corresponding data collapse results are shown in the insets of (e,f), where the horizontal axis label is  $x_{N_B} \equiv (n_B - n_B^{cr})L^{1/\mu}$  where  $n_B \equiv N_B/N$  and  $n_B^{cr} \approx 0.5$ .

tion at  $N_B/N = 1/2$ . This transition is *partition-induced*, as particularly evidenced in Fig. 2(e), where measurement is irrelevant. From the above observations, we infer that the GHZ-entangled phase is confined within the rectangle defined by  $p \leq p_c \approx 0.16$  and  $N_B/N \leq 1/2$ .

The partition-induced phase transition suggests that the GHZ entanglement transition may not be described by a conformal field theory (CFT), as the bipartite entanglement transition with long-range gates [20]. The inconsistency with CFT is corroborated by other evidences. The decomposition (1) implies that  $g = I_{A:B} - 2N_{A,B}$  [53] where  $I_{A:B}$  is mutual information between A and B, and  $N_{A,B} = \log_2 \|\rho_{AB}^T\|_1$  is the entanglement negativity [54] (with  $\rho_{AB}^T$  being the partially transposed reduced density matrix). Meanwhile, for state (1)  $N_{A,B}$  is equivalent to the *computable cross norm negativity* [55]  $\mathcal{E}_{A,B} = \log_2 \|R_{AB}\|_1$  where  $R_{AB}$  “realigns” the elements of the density matrix:  $\langle a, a' | R_{AB} | b, b' \rangle = \langle a, b | \rho_{AB} | a', b' \rangle$ . Both types of negativity, when A and B are adjacent parties, have been evaluated in CFT. However, they do not agree:  $N_{A,B} = \frac{c}{4} \log_2 \frac{l_a l_b}{l_a + l_b} + \text{const.}$  [56] whereas  $\mathcal{E}_{A,B} = \frac{c}{8} [2 \log_2 (l_a l_b) - 3 \log_2 (l_a + l_b)] + \text{const.}$  [57], where  $c$  is the central charge and  $l_i = (N/\pi) \sin(\pi N_i/N)$  with  $i = A, B$ . Further-

more, Ref. [40] proposed a tripartite entanglement measure  $g(A:B) = 2E_P(A:B) - I_{A:B}$  where  $E_P$  is the entanglement of purification [58]. It can be proved that  $g(A:B)$  equals  $g$  when applied to stabilizer states (1). However,  $g(A:B)$  in a CFT is found insensitive to partition, which is incompatible with the strong dependence on partition observed here.

*A quantum Internet perspective.* Evidences of  $\langle g \rangle$  being enhanced by single-qubit measurements can be seen from Figs. 2(b-d). Some of them are finite-size effect within the GHZ-trivial phase. For the GHZ-tangled phase, it is observed from Figs. 2(e,f) that the plateau displayed in Fig. 2(f),  $p = 0.08$ , is higher than that of Fig. 2(e) where  $p = 0$ , by about 0.05. To understand why measurements is not necessarily detrimental, let us map the qubit array into a chain Internet where each qubit, which will be called *atomic* qubit, is located on a node, and a photonic source distributes Bell pairs to the neighboring nodes, as illustrated in Fig. 3(a). The gates between atomic qubits can be realized using the photonic Bell pairs in the manner of quantum teleportation [59], as exemplified by the CNOT gate [60] in Fig. 3(b). Therein, outcomes of the measurements on the photonic qubits must be shared, allowing the other node to control local Z and X operations. However, here communication is un-

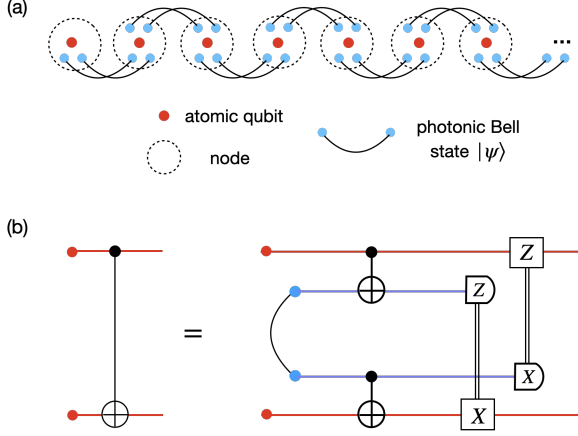


Figure 3. (a) The random circuit can be viewed as a quantum Internet linked in a 1D configuration, where the two-qubit gates are realized by teleportation-based methods. All the operations, unitary or measurements, are implemented locally in each node. (b) Teleported CNOT gate. The circuit needs one photonic Bell pair, local CNOT gates between the atomic and photonic qubits, and local Z or X unitary controlled by the outcome of the remote measurements.

necessary since local Z and X do not affect the sampling of Clifford gates.

Generally, two photonic Bell pairs are sufficient to implement any two-qubit gate [61, 62]. Thus, simulating a random circuit of  $T$  layers is equivalent to distributing  $2T$  Bell pairs for every two neighbors, followed by sequential unitaries and measurements performed locally within each node. We package all the local implementations specified by a trajectory into an operator  $\mathcal{M}_i$  acting on  $2T$  photonic and one atomic qubits. Thus, the final state is expressed as:

$$|\Psi\rangle_T = \bigotimes_{i=1}^N \mathcal{M}_i \circ |\Psi_0\rangle \quad (3)$$

where the resource state contains only Bell type short-range entanglement

$$|\Psi_0\rangle = |0\rangle_1 |\psi\rangle_{1,2}^{\otimes 2T} |0\rangle_2 |\psi\rangle_{2,3}^{\otimes 2T} \cdots |\psi\rangle_{N-1,N}^{\otimes 2T} |0\rangle_N. \quad (4)$$

Now, let us abstract the nature of  $\mathcal{M}_i$  and treat it as a general operator. If  $\mathcal{M}_i$  is unitary, no GHZ-entanglement can be obtained from  $|\Psi\rangle_T$ , because local unitaries do not change anything about entanglement. In this sense, the GHZ-entangled phase obtained without measurement ( $p = 0$ ) effectively arises from measuring the photonic qubits. Thus, it is reasonable that  $\langle g \rangle$  benefits from further measuring some atomic qubits ( $p > 0$ ). This argument indicates that the multipartite entanglement is converted from the fewer-party entanglement. Such theory is currently under development [63].

*GHZ entanglement growth.* At last, we study the growth of  $\langle g \rangle$  for the equal partition  $N_A = N_B = N_C$ . We plot  $\langle g \rangle$  as a function of the circuit layer denoted

by  $t$  (for  $p \in [0, 0.16]$ ) in the upper panel of Fig. 4(a). To illuminate the difference between GHZ entanglement with long-range but bipartite Bell entanglement, we plot parallel results of  $n_{AC}$  in the lower panel of Fig. 4(a). This comparison is intriguing because previous studies of Clifford circuits rely on the *clipped gauge* of the stabilizers [16]. The clipped gauge fails to distinguish the GHZ-entanglement from the Bell-entanglement between A and C, because it records only the first and the last qubit where a stabilizer acts nontrivially, regardless of the supports on B.

The plots show that  $\langle g \rangle$  saturates earlier than  $n_{AC}$ , and there are regimes where constant speed of growth is well-defined, see the insets of Fig. 4(a). The speed of growth of bipartite entanglement is described by the Kardar-Parisi-Zhang equation [16], while that of the GHZ-entanglement is open.  $\langle g \rangle$  grows with a lower speed than  $n_{AC}$ , and slows down when  $p$  is larger. To learn the effect of measurements better, we consider  $p = 0, 0.02, 0.1$  and plot the distribution of the first moment  $t_0$  when  $g$  and  $n_{AC}$  transit to non-zero values in the upper and lower panels of Fig. 4(b), respectively. It shows that a larger  $p$  yields smaller  $t_0$  while flattening the distribution. In addition,  $\min t_0$  of GHZ is visibly smaller, meaning that tripartite GHZ entanglement dominates the A-C bipartite entanglement at early dynamics.

*Conclusions and Discussions.* To summarize, we numerically studied the tripartite GHZ entanglement of the monitored random Clifford circuits and found a GHZ-entangled phase and a GHZ-trivial phase. The transition between them can be measurement-induced at  $p = 0.16$

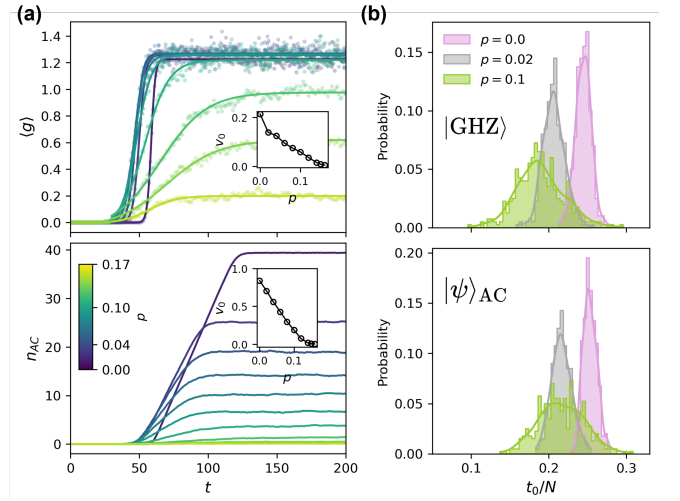


Figure 4. Entanglement growth in the GHZ-entangled phase (equal partition  $N_B = N/3$ ). (a) Values of  $\langle g \rangle$  (upper panel, scattering dots represent the raw data of  $\langle g \rangle$  while the smooth curves are obtained by fitting the data) and  $n_{AC}$  (lower panel) as a function of circuit layer  $t$ . The insets show the speed of growth. (b) The distribution of the first layer  $t_0$  when  $\langle g \rangle$  (upper panel) and  $n_{AC}$  becomes nonzero.



or partition-induced at  $N_B/N = 1/2$ . The partition-induced transition is a new discovery of the multipartite entanglement. We found that GHZ entanglement can be enhanced by measurements. The growth of GHZ entanglement is compared with the growth of long-range bipartite entanglement.

There are questions remain open. Firstly, imagine a phase diagram of  $\langle g \rangle$  akin to Fig. 2(c). Our data is not sufficient to resolve whether the line of  $p = 0.16$  and  $N_B/N > 1/2$  is critical or not. It might be because Fig. 2(d) indicates an unobserved feature: curves of  $\langle g \rangle$  appears concave when  $p < 0.16$  (red) and convex when  $p > 0.16$  (blue), while near  $p_c$  (dashed line) the curve is roughly linear, giving a chance of nonzero  $\langle g \rangle$  for  $N_B/N > 1/2$  in the large  $N$  limit.

Secondly, the partition-induced transition indicates that the relative size matters. Beside that, it is yet to be explored that how the multipartite entanglement depends on the topology of the partitions. For example, let us consider Kitaev's toric code [64] and divide all the qubits into five parties (GHZ state extracted from local junction point [45] is avoided because each stabilizer of the toric code is supported by four qubits). For five-party GHZ entanglement, Eq. (2) still applies [45, 46]. Then  $g \neq 0$  only if there is a logic operator that cannot be cleaned [65] from any party so that it does not belong to  $\cup_\alpha S_{\hat{\alpha}}$ , which requires every party to be topologically nontrivial.

Thanks to Zi-Xiang Li and Run-Ze Chi for useful discussions. Y.-X. Zhang acknowledges the financial support from National Natural Science Foundation of China (Grant No. 12375024), Innovation Program for Quantum Science and Technology (Grant No. 2023ZD0301100 and No. 2-6), CAS Project for Young Scientists in Basic Research (YSBR-100).

---

\* [iyxz@iphy.ac.cn](mailto:iyxz@iphy.ac.cn)

- [1] R. Horodecki, P. Horodecki, M. Horodecki, and K. Horodecki, *Rev. Mod. Phys.* **81**, 865 (2009).
- [2] O. Gühne and G. Tóth, *Physics Reports* **474**, 1 (2009).
- [3] M. Walter, D. Gross, and J. Eisert, *Quantum Information: From Foundations to Quantum Technology Applications*, 293 (2016).
- [4] L. Amico, R. Fazio, A. Osterloh, and V. Vedral, *Rev. Mod. Phys.* **80**, 517 (2008).
- [5] J. Eisert, M. Cramer, and M. B. Plenio, *Reviews of Modern Physics* **82**, 277 (2010).
- [6] N. Laflorencie, *Physics Reports* **646**, 1 (2016).
- [7] D. A. Abanin, E. Altman, I. Bloch, and M. Serbyn, *Reviews of Modern Physics* **91**, 021001 (2019).
- [8] Y. Li, X. Chen, and M. P. A. Fisher, *Phys. Rev. B* **98**, 205136 (2018).
- [9] A. Chan, R. M. Nandkishore, M. Pretko, and G. Smith, *Phys. Rev. B* **99**, 224307 (2019).
- [10] B. Skinner, J. Ruhman, and A. Nahum, *Phys. Rev. X* **9**, 031009 (2019).
- [11] M. Szyniszewski, A. Romito, and H. Schomerus, *Phys. Rev. B* **100**, 064204 (2019).
- [12] M. J. Gullans and D. A. Huse, *Phys. Rev. Lett.* **125**, 070606 (2020).
- [13] Y. Bao, S. Choi, and E. Altman, *Phys. Rev. B* **101**, 104301 (2020).
- [14] C.-M. Jian, Y.-Z. You, R. Vasseur, and A. W. W. Ludwig, *Phys. Rev. B* **101**, 104302 (2020).
- [15] T. Zhou and A. Nahum, *Phys. Rev. B* **99**, 174205 (2019).
- [16] A. Nahum, J. Ruhman, S. Vijay, and J. Haah, *Phys. Rev. X* **7**, 031016 (2017).
- [17] A. Nahum, S. Vijay, and J. Haah, *Phys. Rev. X* **8**, 021014 (2018).
- [18] Y. Li, S. Vijay, and M. P. Fisher, *PRX Quantum* **4**, 010331 (2023).
- [19] A. Nahum, S. Roy, B. Skinner, and J. Ruhman, *PRX Quantum* **2**, 010352 (2021).
- [20] M. Block, Y. Bao, S. Choi, E. Altman, and N. Y. Yao, *Phys. Rev. Lett.* **128**, 010604 (2022).
- [21] S. Sharma, X. Turkeshi, R. Fazio, and M. Dalmonte, *SciPost Phys. Core* **5**, 023 (2022).
- [22] A. Lavasani, Y. Alavirad, and M. Barkeshli, *Phys. Rev. Lett.* **127**, 235701 (2021).
- [23] A. Lavasani, Y. Alavirad, and M. Barkeshli, *Nature Physics* **17**, 342 (2021).
- [24] X. Turkeshi, R. Fazio, and M. Dalmonte, *Phys. Rev. B* **102**, 014315 (2020).
- [25] P. Sierant, M. Schirò, M. Lewenstein, and X. Turkeshi, *Phys. Rev. B* **106**, 214316 (2022).
- [26] H. Liu, T. Zhou, and X. Chen, *Phys. Rev. B* **106**, 144311 (2022).
- [27] X. Feng, B. Skinner, and A. Nahum, *PRX Quantum* **4**, 030333 (2023).
- [28] S.-K. Jian, C. Liu, X. Chen, B. Swingle, and P. Zhang, *Phys. Rev. Lett.* **127**, 140601 (2021).
- [29] M. Ippoliti and V. Khemani, *Phys. Rev. Lett.* **126**, 060501 (2021).
- [30] T.-C. Lu and T. Grover, *PRX Quantum* **2**, 040319 (2021).
- [31] M. Ippoliti, T. Rakovszky, and V. Khemani, *Phys. Rev. X* **12**, 011045 (2022).
- [32] S. Choi, Y. Bao, X.-L. Qi, and E. Altman, *Phys. Rev. Lett.* **125**, 030505 (2020).
- [33] M. J. Gullans, S. Krastanov, D. A. Huse, L. Jiang, and S. T. Flammia, *Phys. Rev. X* **11**, 031066 (2021).
- [34] R. Fan, S. Vijay, A. Vishwanath, and Y.-Z. You, *Phys. Rev. B* **103**, 174309 (2021).
- [35] Y. Li and M. P. A. Fisher, *Phys. Rev. B* **103**, 104306 (2021).
- [36] Z. Weinstein, Y. Bao, and E. Altman, *Phys. Rev. Lett.* **129**, 080501 (2022).
- [37] S. Liu, M.-R. Li, S.-X. Zhang, S.-K. Jian, and H. Yao, *Phys. Rev. B* **107**, L201113 (2023).
- [38] S. Liu, M.-R. Li, S.-X. Zhang, and S.-K. Jian, *Phys. Rev. Lett.* **132**, 240402 (2024).
- [39] J. C. Hoke, M. Ippoliti, E. Rosenberg, D. Abanin, R. Acharya, T. I. Andersen, M. Ansmann, F. Arute, K. Arya, A. Asfaw, J. Atalaya, J. C. Bardin, A. Bengtsson, G. Bortoli, A. Bourassa, J. Bovaird, L. Brill, M. Broughton, B. B. Buckley, D. A. Buell, T. Burger, B. Burkett, N. Bushnell, Z. Chen, B. Chiaro, D. Chik, J. Cogan, R. Collins, P. Conner, W. Courtney, A. L. Crook, B. Curtin, A. G. Dau, D. M. Debroy, A. Del Toro Barba, S. Demura, A. Di Paolo, I. K. Droz-

- dov, A. Dunsworth, D. Eppens, C. Erickson, E. Farhi, R. Fatemi, V. S. Ferreira, L. F. Burgos, E. Forati, A. G. Fowler, B. Foxen, W. Giang, C. Gidney, D. Gilboa, M. Giustina, R. Gosula, J. A. Gross, S. Habegger, M. C. Hamilton, M. Hansen, M. P. Harrigan, S. D. Harrington, P. Heu, M. R. Hoffmann, S. Hong, T. Huang, A. Huff, W. J. Huggins, S. V. Isakov, J. Iveland, E. Jeffrey, Z. Jiang, C. Jones, P. Juhás, D. Kafri, K. Kechedzhi, T. Khattar, M. Khezri, M. Kieferová, S. Kim, A. Kitaev, P. V. Klimov, A. R. Klots, A. N. Korotkov, F. Kostritsa, J. M. Kreikebaum, D. Landhuis, P. Laptev, K.-M. Lau, L. Laws, J. Lee, K. W. Lee, Y. D. Lensky, B. J. Lester, A. T. Lill, W. Liu, A. Locharla, O. Martin, J. R. McClean, M. McEwen, K. C. Miao, A. Mieszala, S. Montazeri, A. Morvan, R. Movassagh, W. Mruczkiewicz, M. Neeley, C. Neill, A. Nersisyan, M. Newman, J. H. Ng, A. Nguyen, M. Nguyen, M. Y. Niu, T. E. O’Brien, S. Omonije, A. Opremcak, A. Petukhov, R. Potter, L. P. Pryadko, C. Quintana, C. Rocque, N. C. Rubin, N. Saei, D. Sank, K. Sankaragomathi, K. J. Satzinger, H. F. Schurkus, C. Schuster, M. J. Shearn, A. Shorter, N. Shutty, V. Shvarts, J. Skrzny, W. C. Smith, R. Somma, G. Sterling, D. Strain, M. Szalay, A. Torres, G. Vidal, B. Villalonga, C. V. Heidweiller, T. White, B. W. K. Woo, C. Xing, Z. J. Yao, P. Yeh, J. Yoo, G. Young, A. Zalcman, Y. Zhang, N. Zhu, N. Zobrist, H. Neven, R. Babbush, D. Bacon, S. Boixo, J. Hilton, E. Lucero, A. Megrant, J. Kelly, Y. Chen, V. Smelyanskiy, X. Mi, V. Khemani, P. Roushan, and Google Quantum AI and Collaborators, *Nature* **622**, 481 (2023).
- [40] Y. Zou, K. Siva, T. Soejima, R. S. K. Mong, and M. P. Zaletel, *Phys. Rev. Lett.* **126**, 120501 (2021).
- [41] S. Nezami and M. Walter, *Phys. Rev. Lett.* **125**, 241602 (2020).
- [42] D. Gottesman, “The heisenberg representation of quantum computers,” (1998), [arXiv:quant-ph/9807006 \[quant-ph\]](https://arxiv.org/abs/quant-ph/9807006).
- [43] S. Aaronson and D. Gottesman, *Phys. Rev. A* **70**, 052328 (2004).
- [44] S. Anders and H. J. Briegel, *Phys. Rev. A* **73**, 022334 (2006).
- [45] S. Bravyi, D. Fattal, and D. Gottesman, *Journal of Mathematical Physics* **47** (2006).
- [46] D. Fattal, T. S. Cubitt, Y. Yamamoto, S. Bravyi, and I. L. Chuang, “Entanglement in the stabilizer formalism,” (2004), [arXiv:quant-ph/0406168 \[quant-ph\]](https://arxiv.org/abs/quant-ph/0406168).
- [47] S. J. Avakian, T. Pereg-Barnea, and W. Witczak-Krempa, “Long-range multipartite entanglement near measurement-induced transitions,” (2024), [arXiv:2404.16095 \[quant-ph\]](https://arxiv.org/abs/2404.16095).
- [48] G. Smith and D. Leung, *Phys. Rev. A* **74**, 062314 (2006).
- [49] *Supplemental Material*.
- [50] M. J. Gullans and D. A. Huse, *Phys. Rev. X* **10**, 041020 (2020).
- [51] M. A. Nielsen and I. L. Chuang, *Quantum Computation and Quantum Information: 10th Anniversary Edition* (Cambridge University Press, 2010).
- [52] Y. Li, X. Chen, and M. P. A. Fisher, *Phys. Rev. B* **100**, 134306 (2019).
- [53] S. Sang, Y. Li, T. Zhou, X. Chen, T. H. Hsieh, and M. P. Fisher, *PRX Quantum* **2**, 030313 (2021).
- [54] G. Vidal and R. F. Werner, *Phys. Rev. A* **65**, 032314 (2002).
- [55] K. Chen and L.-A. Wu, *Quantum Information and Computation* **3**, 193 (2003).
- [56] P. Calabrese, J. Cardy, and E. Tonni, *Phys. Rev. Lett.* **109**, 130502 (2012).
- [57] C. Yin and Z. Liu, *Phys. Rev. Lett.* **130**, 131601 (2023).
- [58] B. M. Terhal, M. Horodecki, D. W. Leung, and D. P. DiVincenzo, *Journal of Mathematical Physics* **43**, 4286 (2002), [https://pubs.aip.org/aip/jmp/article-pdf/43/9/4286/19183123/4286\\_1\\_online.pdf](https://pubs.aip.org/aip/jmp/article-pdf/43/9/4286/19183123/4286_1_online.pdf).
- [59] C. H. Bennett, G. Brassard, C. Crépeau, R. Jozsa, A. Peres, and W. K. Wootters, *Phys. Rev. Lett.* **70**, 1895 (1993).
- [60] K. S. Chou, J. Z. Blumoff, C. S. Wang, P. C. Reinhold, C. J. Axline, Y. Y. Gao, L. Frunzio, M. H. Devoret, L. Jiang, and R. J. Schoelkopf, *Nature* **561**, 368 (2018).
- [61] J. Eisert, K. Jacobs, P. Papadopoulos, and M. B. Plenio, *Phys. Rev. A* **62**, 052317 (2000).
- [62] D. Collins, N. Linden, and S. Popescu, *Phys. Rev. A* **64**, 032302 (2001).
- [63] J. de Jong, F. Hahn, N. Tcholchev, M. Hauswirth, and A. Pappa, *Phys. Rev. Res.* **6**, 013330 (2024).
- [64] A. Kitaev, *Annals of Physics* **303**, 2 (2003).
- [65] S. Bravyi and B. Terhal, *New Journal of Physics* **11**, 043029 (2009).



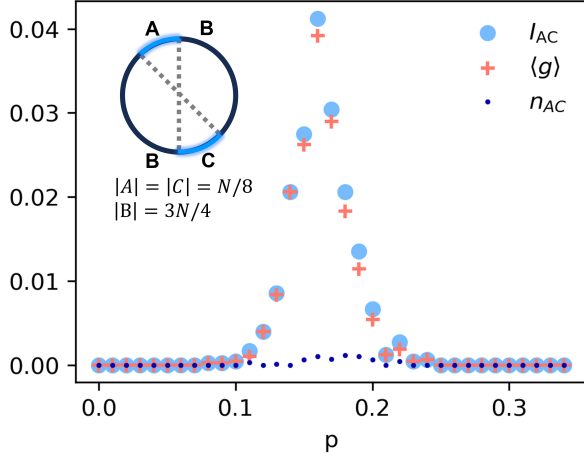


FIG. S2. Calculations of the mutual information  $I_{AC}$ , following Fig. 7 of Ref. [R1], GHZ index  $\langle g \rangle$ , and the amount of A-C bipartite entanglement  $n_{AC}$  of the configuration shown in the inset. The periodic boundary condition is applied and the partition reads  $|A| = |C| = N/8$  and  $B$  contains two disjoint sections with the total number  $|B| = 3N/4$ .

where  $T_B$  denotes the partial transpose on the subsystem  $B$ ,  $S(A)$  represents the von Neumann entropy of subsystem  $A$  and similarly to  $S(B)$  and  $S(C)$ . Recall that a stabilizer state  $\rho$  is generated from the product state by a Clifford unitary  $U$ . We express the dependence of  $\rho$  on  $U$  implicitly, so that the expectation value of  $g$  averaged over the  $N$ -qubit Clifford group reads

$$\langle g \rangle = \frac{1}{\mathcal{N}} \sum_U \left( \log_2(\text{Tr}[(\rho_{AB}^{T_B})^3]) + S(A) + S(B) + S(C) \right), \quad (\text{Q3})$$

where  $\mathcal{N}$  denotes the size of the  $N$ -qubit Clifford group. For the logarithmic term, the Jensen inequality of concave function  $\log_2(x)$  indicates that

$$\frac{1}{\mathcal{N}} \sum_U \log_2(\text{Tr}[(\rho_{AB}^{T_B})^3]) \leq \log_2 \left( \frac{1}{\mathcal{N}} \sum_U \text{Tr}[(\rho_{AB}^{T_B})^3] \right). \quad (\text{Q4})$$

To linearize the formula, we apply the triple replica trick through two permutation operators  $R_A^+$  and  $R_B^-$  acting on three copies of  $\rho_A$  and  $\rho_B$ , respectively,

$$\begin{aligned} \frac{1}{\mathcal{N}} \sum_U \text{Tr}[(\rho_{AB}^{T_B})^3] &= \frac{1}{\mathcal{N}} \sum_U \text{Tr}[\rho_{AB}^{\otimes 3} R_A^+ R_B^-] \\ &= \text{Tr} \left[ \left( \frac{1}{\mathcal{N}} \sum_U \rho^{\otimes 3} \right) R_A^+ R_B^- \right] \end{aligned} \quad (\text{Q5})$$

Operator  $R_A^+$  permutes the Hilbert spaces of the three copies according to  $|k\rangle_1 \rightarrow |k\rangle_2 \rightarrow |k\rangle_3 \rightarrow |k\rangle_1$  for every

basis state  $|k\rangle$ .  $R_B^-$  works similarly but on the opposite direction  $|k\rangle_1 \rightarrow |k\rangle_3 \rightarrow |k\rangle_2 \rightarrow |k\rangle_1$ .

As the multiqubit stabilizer states are projective 3-designs[R3, R4], The average of the states can be written as the summation of permutation operators with equal coefficients,

$$\frac{1}{\mathcal{N}} \sum_U \rho^{\otimes 3} = \frac{1}{\alpha} \sum_{\pi=0}^5 \rho_{\pi} \quad (\text{Q6})$$

$$\rho_0 = \mathbf{1} \quad (\text{Q7})$$

$$\rho_1 = \text{SWAP}_{12} \otimes \mathbf{1}_3 \quad (\text{Q8})$$

$$\rho_2 = \text{SWAP}_{23} \otimes \mathbf{1}_1 \quad (\text{Q9})$$

$$\rho_3 = \text{SWAP}_{13} \otimes \mathbf{1}_2 \quad (\text{Q10})$$

$$\rho_4 = \rho_1 \rho_2 \quad (\text{Q11})$$

$$\rho_5 = \rho_2 \rho_1 \quad (\text{Q12})$$

where  $\alpha = d(d+1)(d+2)$ ,  $d = 2^N$  and  $N$  is the system size. The trace of permutation operators  $\text{Tr}\{\rho_0\} = 2^{3 \cdot N}$ ,  $\text{Tr}\{\rho_1\} = \text{Tr}\{\rho_2\} = \text{Tr}\{\rho_3\} = 2^{2 \cdot N}$ ,  $\text{Tr}\{\rho_4\} = \text{Tr}\{\rho_5\} = 2^N$ . A straightforward insight at these results is that the trace of a general "SWAP" gate is the number of invariant states. So, SWAP between two copies has the invariant states  $|\phi_{\mu}\rangle_1 \otimes |\phi_{\mu}\rangle_2$ , where  $\mu \in [1, 2^{d_{\phi}}]$ .  $\text{Tr}\{\text{SWAP}_{12}\} = 2^N$ . The general SWAP between three copies shares the same nature while invariant states are  $|\phi_{\mu}\rangle_1 \otimes |\phi_{\mu}\rangle_2 \otimes |\phi_{\mu}\rangle_3$ . The subscriptions of SWAP represent the copies of the density matrix.

In this notation, the permutations  $R_A^+$  and  $R_B^-$  of subsystem (A,B,C) among different copies (1,2,3) can be written as,

$$R_A(+)= (\text{SWAP}_{12}^A \otimes \mathbf{1}_3^A)(\mathbf{1}_1^A \otimes \text{SWAP}_{23}^A) \otimes \mathbf{1}_{123}^B \otimes \mathbf{1}_{123}^C \quad (\text{Q13})$$

$$R_B(-)= \mathbf{1}_{123}^A \otimes (\mathbf{1}_1^B \otimes \text{SWAP}_{23}^B)(\text{SWAP}_{12}^B \otimes \mathbf{1}_3^B) \otimes \mathbf{1}_{123}^C \quad (\text{Q14})$$

For the trace of each terms of  $\rho_{\pi} R_A(+)\rho_{\pi} R_B(-)$ ,

$$\begin{aligned} \text{Tr}[\rho_0 R_A(+)\rho_0 R_B(-)] &= \text{Tr}[R_A(+)\rho_0 R_B(-)] \\ &= \text{Tr} \left( (\text{SWAP}_{12}^A \otimes \mathbf{1}_3^A)(\mathbf{1}_1^A \otimes \text{SWAP}_{23}^A) \right. \\ &\quad \left. \otimes (\mathbf{1}_1^B \otimes \text{SWAP}_{23}^B)(\text{SWAP}_{12}^B \otimes \mathbf{1}_3^B) \mathbf{1}_{123}^C \right) \\ &= 2^{N_A} \cdot 2^{N_B} \cdot 2^{3N_C} = 2^{N+2N_C} \end{aligned} \quad (\text{Q15})$$



Similarly, we obtain that

$$\text{Tr}\{\rho_1 R_A(+)\rho_2 R_B(-)\} = 2^{2N_A} \cdot 2^{2N_B} \cdot 2^{2N_C} = 2^{2N} \quad (\text{Q16})$$

$$\text{Tr}\{\rho_2 R_A(+)\rho_3 R_B(-)\} = 2^{2N_A} \cdot 2^{2N_B} \cdot 2^{2N_C} = 2^{2N} \quad (\text{Q17})$$

$$\text{Tr}\{\rho_3 R_A(+)\rho_4 R_B(-)\} = 2^{2N_A} \cdot 2^{2N_B} \cdot 2^{2N_C} = 2^{2N} \quad (\text{Q18})$$

$$\text{Tr}\{\rho_4 R_A(+)\rho_5 R_B(-)\} = 2^{N_A} \cdot 2^{3N_B} \cdot 2^{N_C} = 2^{N+2N_B} \quad (\text{Q19})$$

$$\text{Tr}\{\rho_5 R_A(+)\rho_1 R_B(-)\} = 2^{3N_A} \cdot 2^{N_B} \cdot 2^{N_C} = 2^{N+2N_A} \quad (\text{Q20})$$

So the Haar average in  $\langle g \rangle$ , i.e., Eq.(Q5), is

$$\begin{aligned} \text{Eq. (Q5)} &= \frac{1}{\alpha} (2^N (2^{2N_A} + 2^{2N_B} + 2^{2N_C}) + 3 * 2^{2N}) \\ &= \frac{3 * 2^{2N} + 2^N (2^{2N_A} + 2^{2N_B} + 2^{2N_C})}{(2^N)(2^N + 1)(2^N + 2)} \\ &< \frac{3}{2^N} + \frac{2^{2N_A} + 2^{2N_B} + 2^{2N_C}}{(2^N + 1)(2^N + 2)} \quad (\text{Q21}) \end{aligned}$$

For an equally tripartite system ( $N_A = N_B = N_C = 1/3N$ ) the upper bound of the logarithmic term in the thermal limit is then:

$$\lim_{N \gg 1} \frac{3}{2^N} + \frac{2^{2N_A} + 2^{2N_B} + 2^{2N_C}}{(2^N + 1)(2^N + 2)} = \frac{3}{2^N} \quad (\text{Q22})$$

Together with Eq. (Q3) and Eq. (Q4), we obtain an upper bound of  $\langle g \rangle$ ,

$$\begin{aligned} \langle g \rangle &< \log_2\left(\frac{3}{2^N}\right) + S(A) + S(B) + S(C) \\ &= \log_2(3) - N + S(A) + S(B) + S(C) \\ &< \log_2(3) \quad (\text{Q23}) \end{aligned}$$

- 
- [R1] Y. Li, X. Chen, and M. P. A. Fisher, *Phys. Rev. B* **100**, 134306 (2019).  
[R2] S. Nezami and M. Walter, *Phys. Rev. Lett.* **125**, 241602 (2020).

- [R3] H. Zhu, *Phys. Rev. A* **96**, 062336 (2017).  
[R4] Z. Webb, *Quant. Inf. Comput.* **16**, 1379 (2016), arXiv:1510.02769 [quant-ph].